Investigation on Structural Build-Up of 3D Printable Foam Concrete

Viacheslav Markin(✉), Irina Ivanova, Shirin Fataei, Silvia Reißig, and Viktor Mechtcherine

Institute of Construction Materials, TU Dresden, Dresden, Germany
viacheslav.markin@tu-dresden.de

Abstract. Over the last decade the use of foam concrete in the construction industry has become popular due to its high thermal and acoustic insulation capacity in combination with sufficient strength characteristics. The use of foam concrete in 3D printing (3D Foam Concrete Printing) is a perspective approach which should enable automated freeform construction without formwork and at the same time would contribute to sustainability and energy efficiency of the structures. Since 3D-printing requires very specific rheological properties of foam concrete in its fresh state, a systematic research on this subject is needed. For this purpose, foam concrete mixtures containing more than 35 vol% protein-based foam and fresh density of approx. 1200 kg/m^3 were developed and investigated with respect to their suitability for 3D printing by extrusion-based selective material deposition. Constant shear rate rheometer tests were performed to determine static yield stress and critical strain at flow onset at concrete ages of 30 min to 150 min, the time interval specifically relevant for the 3D printing process. Finally, the estimation of structural build-up was verified by manufacturing 800 mm long foam concrete walls until their collapse.

Keywords: 3D-printing · Foam concrete · Rheology · Digital construction · Thixotropy

1 Introduction

Formwork-free digital concrete (DC) construction methods such as 3D concrete printing have showed their high potentials for increasing productivity on the construction site [1–4]. The variety of the research topics, challenges and opportunities in the context of DC was well summarised in [5]. The research at hand focusses on a novel approach of using foam concrete in extrusion-based 3D printing.

Foam concrete (FC) is a lightweight material, which can be produced by pre-foaming or mixed foaming [6] with a range of densities down to 400 kg/m^3 [7, 8]. As a result of its low density, FC yields high thermal insulation capacity. Typical characteristics of modern foam concretes are reported in [8, 9].

The variety of foaming techniques and methods for intermixing the foam into the cement-based matrix enables the production of foam concrete to be adapted for a continuous DC processing. Some production techniques for printable foam concrete and feeding systems for 3D printing are described in [10]. The concept of mixture

F. P. Bos et al. (Eds.): DC 2020, RILEM Bookseries 28, pp. 301–311, 2020.
https://doi.org/10.1007/978-3-030-49916-7_31

design for printable foam concrete was developed in the framework of the CONPrint3D-Ultralight® project; the obtained print experiments proved the possibility of additive fabrication with foam concrete [11]. In a further research at the TU Dresden, printable foam concrete with density as low as 860 kg/m^3 and compressive strength of 2.5 MPa at an age of 14 days was produced [12].

The research at hand deals with rheological properties of printable foam concrete. The main rheological characteristics of fresh FC – static and dynamic yield stresses, modulus of elasticity and structuration rate – were determined by means of constant shear rate (CSR) test on foam concretes made of different raw materials. To estimate the maximum numbers of layers which can be deposited on upon other before structural failure of the wall occurs, we assumed that the collapse takes place due to the deformation in the first wall layer upon reaching static yield stress, thus, neglecting buckling propensity. Therefore, for prediction of the critical number of printed layers, the theoretically estimated static yield stress in the bottom layer was compared to the static yield stress defined by a rheometry test. The influence of the geometrical factor α_{geom} described in [13, 14] was neglected. Furthermore, the predicted buildability of FC was compared to the actual printing test results. To ensure comparability, the rheological measurements were performed simultaneously with the printing experiments on the same FC batches.

2 Experimental Program

2.1 Materials and Mixture Proportions

Table 1 presents compositions of the investigated foam concretes. The binder of all compositions contains a type II Portland composite cement CEM II/A-M (S-LL) 52.5 R (OPTERRA Zement GmbH, Werk Karsdorf, Germany) and hard coal fly ash Steament H-4 (STEAG Power Minerals GmbH, Dinslaken, Germany). As further pozzolanic additives silica fume (Grade 971U, Elkem ASA Silicon Materials, Skøyen, Norway) and alumosilicate (Centrilit NC II, MC-Bauchemie GmbH & Co. KG, Bottrop, Germany) were used. The chemical composition of the materials is given in Table 2.

A protein-based foaming agent (Oxal PLB6, MC-Bauchemie GmbH & Co. KG, Bottrop, Germany) was diluted with water in the ratio 1:30 (by volume) and then utilized for production of the foam with an average density of 60 kg/m^3. Technical characteristics of used foam generator and settings for production of foam are described in [12]. Polycarboxylate ether-based superplasticizers MasterGlenium SKY 593 (BASF Construction Solutions GmbH, Trostberg, Germany) and MC-PowerFlow 5100 (MC-Bauchemie Müller GmbH & Co. KG, Bottrop, Germany) were used for achieving the required workability and reducing the water content.

Table 1. Mixture compositions in accordance with design guidelines for printable foam concretes in [11]. The percentages of the total volume in the binder are shown in brackets.

Material	M-A1	M-A2	M-A3
Cement [kg]	626 (60 vol%)	559 (55 vol%)	564 (55 vol%)
Fly ash [kg]	297 (40 vol%)	290 (40 vol%)	292 (40 vol%)
Water [l]	251	288	275
Superplastisizer [l]	0.002	0.0027	0.002
Silica fume [kg]	–	37 (5 vol%)	–
Alumosilicate [kg]	–	–	43 (5 vol%)
Foam [l]	41	38	39
FC $(w/z)_{eq}$	0.37	0.44	0.41
Design density [kg/m^3]	1200	1200	1200
Plastic density after extrusion [kg/m^3]	1140	1066	1246

Table 2. Chemical composition of raw materials used for FC (LOI: loss on ignition, n.d.: not determined).

Material	Density [g/cm^3]	Chemical composition [% by mass]											
		Residue	SiO_2	Al_2O_3	Fe_2O_3	CaO	MgO	SO_3	K_2O	Na_2O	LOI	CO_2	CL
Cement	3.12	0.74	20.63	5.35	2.82	60.9	2.14	3.52	1.05	0.22	3.47	2.8	0.07
Fly ash	2.22	n.d.	n.d.	n.d.	n.d.	3.6	n.d.	0.6	n.d.	2.9	1.8	n.d.	0.01
$Al_2SiO_5^*$	2.61	n.d.	51.2	44.9	n.d.	n.d.	n.d.	n.d.	1.0	n.d.	n.d.	n.d.	n.d.
Silica fume	2.29	n.d.	98.4	0.20	0.01	0.20	0.10	0.10	0.20	0.15	0.50	n.d.	0.01

*Alumosilicate

2.2 Mixture Preparation

The mixing of the components took place in the cone mixer KKM 30L [15]. The mixture was designed for a total volume of 30 L. The mixing process was subdivided into two steps: (1) mixing of the cement-based matrix and (2) intermixing of the prefabricated foam into the cement-based matrix. At first, dry materials were homogenized for 2 min with an engine speed of 3000 rpm. Subsequently, water and superplasticizer were added, and the mixing was resumed for further 2 min at the same speed. In the next step, the speed was reduced to 1500 rpm and the separately prepared foam was gradually added. To avoid damage to the foam structure caused by overexposure to mechanical stirring, the mixing time for each portion of the foam was kept below 30 s. The blending of the foam took in total 5 min.

2.3 Rheometry

HAAKE MARS II Rheometer was used with building materials cell and vane configuration. Temperature of the samples was maintained at 20 °C during testing.

Determination of Bingham parameters was conducted as follows: 10 rotational steps from 0.1 s^{-1} to 10 s^{-1} in 30 s, rotation at 10 s^{-1} for 30 s, 15 rotational steps from 10 s^{-1} to 0.1 s^{-1} in 45 s. This stage was also used as pre-shear, which was performed to ensure similar state of the samples before static rheological measurements.

Static yield stress (SYS) values were determined by means of CSR test [16, 17] using single-batch approach [18]. Test duration was set to 240 s; each SYS measurement was manually interrupted when the peak values of shear stress were reached. In order to study the effect of CSR on the obtained values of the SYS, different CSRs of 0.08, 0.12, 0.15, and 0.18 s^{-1} were applied. Structuration rate was estimated using Roussel's model [19].

2.4 The 3D Printing Process

3D printing with the designed mix compositions was conducted using custom developed 3D printing testing device (3DPTD) earlier described in [11]. 3DPTD was equipped with a progressive cavity screw and a rectangular nozzle with an opening of 14 mm × 33 mm. The printhead was moving at a constant speed of 40 mm/s. Straight wall specimens with a length of 800 mm were produced with layer-to-layer deposition time intervals (*TI*) of 2 min, 5 min and 10 min. Deposition of the layers was aborted after collapse of the wall specimens or inability to print because of, e.g., overstiffening of the material. The number of printed layers before the occurrence of noticeable deformations and collapse of the wall was recorded.

3 Results and Discussion

3.1 Bingham Parameters

Figure 1 presents the dynamic yield stress values for three different foam concretes. In comparison to the composition M-A2 with dynamic yield stress of approximately 320 Pa, composition M-A1 demonstrated higher dynamic yield stress of 355 Pa, while the highest dynamic yield stress of 388 Pa was observed for composition M-A3. These differences can be traced back to the various composition of the binder used. According to the results in Fig. 1, composition M-A2 is more suitable for pumping since its plastic viscosity (approximately 6.4 Pa s) is lower than for compositions M-A1 and M-A3 (approximately 9.6 Pa s). On the other hand, to assure shape stability just after extrusion, higher dynamic yield stress is advantageous [20]. This opportune characteristic is attributive to composition M-A3.

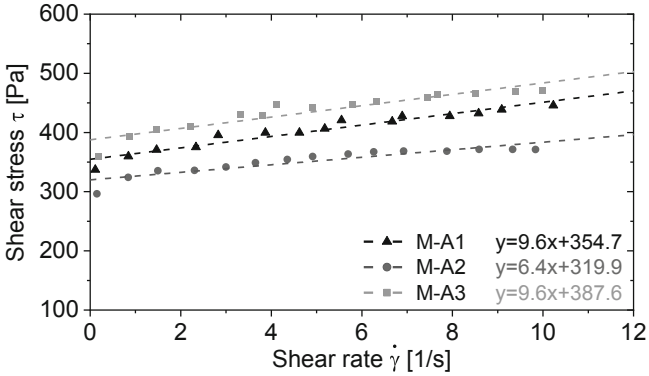

Fig. 1. Flow curves of the foam concrete under investigation.

3.2 Selecting Constant Shear Rate for Static Yield Stress Measurements

Figure 2 illustrates the effect of the applied CSR on the shear stress development over time for the foam concrete composition M-A1 at the age of approximately 40 min after adding water. It is worth noting that different testing times were required to reach the peak values by applying different shear rates on the foam concrete sample. It could be also observed that the value of the SYS depends on the shear rate used in the experiment, while the maximum value of shear stress could be reached faster by applying higher shear rate.

During pumping and deposition of the foam concrete layers, the material is sheared most intensively. However, after deposition, foam concrete layers remain mainly in a resting state, which leads to the inference that the material should be tested at a lowest possible CSR to simulate this static condition. Experimental results showed that by applying CSR of 0.08 s^{-1} even at the age of 150 min after water addition, flow onset could be reached within a reasonable testing time of 180 s. Considering this result and the findings in [17], CSR of 0.08 s^{-1} was chosen for further investigation.

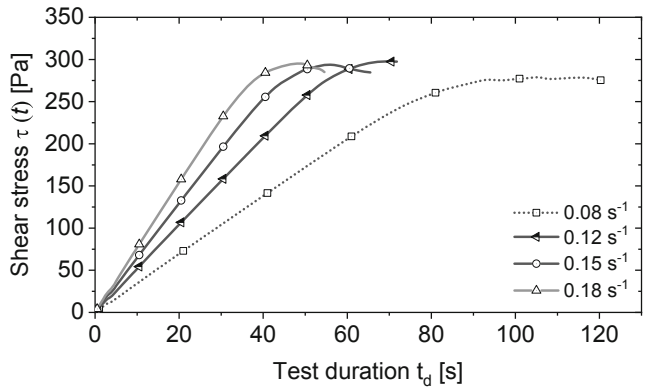

Fig. 2. Influence of the applied constant shear rate on the development of the shear stress over the time of the foam concrete sample M-A1.

3.3 Structuration Rate

Figure 3 shows the development of the shear stress of composition M-A1 with time after water addition. SYS τ_0 increased with the resting time t_{rest}, while shear strain γ decreased. Compositions M-A2 and M-A3 demonstrated a similar dependence of the SYS on resting time. It was also determined that shear elastic modulus *G(t)* increased with a magnitude corresponding to the τ_c and t_{rest} values.

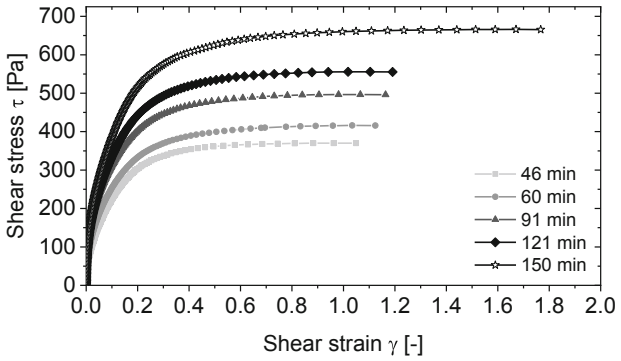

Fig. 3. Shear stress-shear strain curves for composition M-A1 at various times after mixing.

Within the investigated period, all three foam concrete compositions exhibited linear growth in SYS over time, which complies to Roussel's model described in [19]; see Fig. 4. The slope of the dashed lines gives a value of the structuration rate of the material, also referred to as A_{thix}. Compositions M-A2 and M-A3 showed structuration rate of 4.6 Pa/min and 4.9 Pa/min, respectively, which is pronouncedly higher than the structuration rate of 2.7 Pa/min as seen with composition M-A1. Obviously, very fine pozzolanic additives silica fume and alumosilicate in compositions M-A2 and M-A3, respectively, accelerated the flocculation/hydration processes.

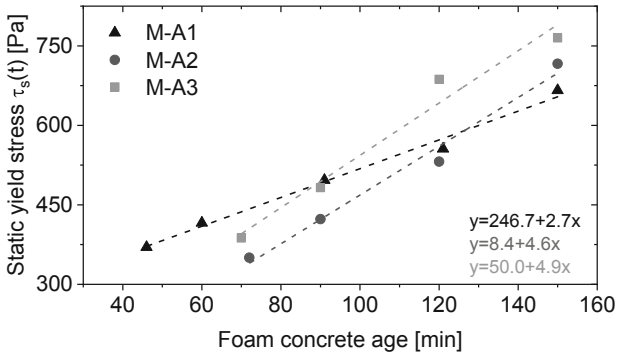

Fig. 4. Development of the static yield stress in time.

It should be noted that the material behaviour was only investigated within the first 150 min after water addition. Eventually, a shift from linear to exponential development of the structuration rate is expected with progressing hydration. Using A_{thix} values, the building rate of foam concrete walls, at which layers can support themselves and the weight of subsequent layers, could be determined; see Sect. 3.5.

3.4 Printing Test

All three foam concrete compositions could be extruded and deposited in layers. However, printing characteristics of each composition differed. Thus, for all examined foam concrete wall specimens with *TI* of 2 min, approximately 7 layers could be printed before noticeable deformations and final collapse of the wall specimen occurred.

With *TI* of 5 min, none of the wall specimens collapsed. The critical number of layers could not been reached because of overstiffening of the material. It is worth noting that blockage of the nozzle did not occur, rather the surface quality decreased and certain discontinuities in the printed layers appeared. Figure 5 depicts the printed wall specimen with foam concrete M-A1 consisting of 25 layers. The last layer was printed at the age of 247 min after water addition. Thus, the entire printing of the wall specimen took 135 min. It could be seen that the surface quality of the layers decreases with the increase in wall height; see Fig. 5b. Using compositions M-A2 and M-A3, 16 and 14 layers, respectively, could be printed, until the experiment was stopped.

Wall specimens produced with *TI* of 10 min suffered from the pronounced stiffening of the mixture. With the composition M-A1, only 15 layers could be printed, while the number decreased to just 7 layers for the compositions M-A2 and M-A3.

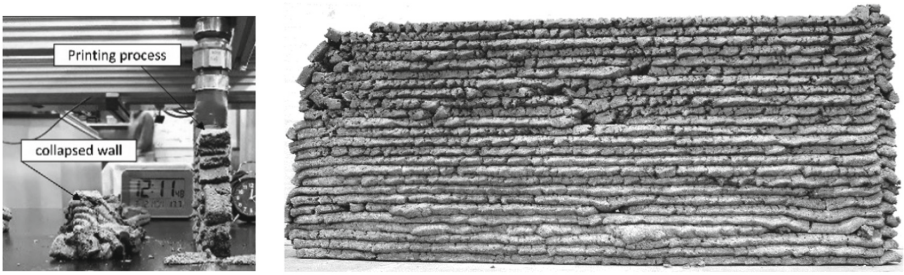

Fig. 5. 3D printing of the foam concrete M-A1: (a) collapsed wall with *TI* of 2 min and upright standing wall being printed with *TI* of 5 min *TI*; (b) foam concrete wall specimen printed with *TI* of 5 min.

3.5 Comparison of the Theoretically and Experimentally Obtained Results

By applying the foam concrete density ρ, measured directly after extrusion, layer height h, defined by nozzle shape, and gravity constant g in Eq. (1), the theoretical SYS in the bottom layer can be calculated by:

$$\tau_0 = \frac{\rho g h}{\sqrt{3}} \tag{1}$$

Subsequently, the theoretical SYS in the bottom layer depending on the number of printed layers was computed using Eq. (2):

$$\tau_{0,f} = \frac{\rho g H_m}{\sqrt{3}} \tag{2}$$

where H_m is the height of the wall specimen. The required SYS depending on the number of printed layers can be expressed with:

$$\tau_{0,f} = \tau_0 + A_{thix} \cdot TI \cdot (n_t - 1) \tag{3}$$

where τ_0 is initial critical SYS, A_{thix} is structuration rate of the material, TI is time interval between layers, and n_t is total number of printed layers. Note, that in Eq. (3), time for printing of the single layer, which depends on the printing velocity, is ignored, since it is negligibly small in comparison to the duration between printing of subsequent layers.

Figure 6 presents the results of the theoretically determined required yield stress in the bottom layer for printing the wall specimen using composition M-A1 and effective yield stress in the bottom layer by applying experimentally determined rheological parameters in Eq. (3).

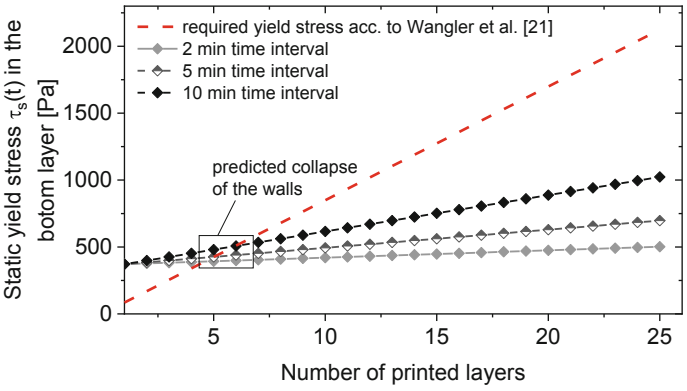

Fig. 6. Prediction of the foam concrete wall stability based on a theoretical calculation and a calculation using experimentally determined rheological parameters; results for the foam concrete M-A1.

The intersection of the red-dashed line acc. to Eq. (2) with other lines shows when the theoretical threshold of the SYS is reached and structural collapse is to be expected. Therefore, for a wall printed with *TIs* of 2 min and 5 min, critical deformations leading to the collapse of the wall should be reached at layer number 5. Whereby, by extending the *TI* to 10 min, collapse of the wall is expected after the printing 7 layers. It is worth noting that theoretical calculation using Eq. (2) and calculation using Eq. (3), which contains experimentally determined rheological values, differ from the results gained by the direct printing test. Hypothetically, this discrepancy occurred due to different drying kinetics of the material in the rheometer cell and during the printing experiment. In the case of foam concrete, this effect can be more pronounced owing to its higher pore surface area in comparison with conventional concrete. Only the prediction for the wall specimens with *TI* of 2 min is in accordance with the results of the 3D printing test.

The results for compositions M-A2 and M-A3 differ from composition M-A1 in the first stage, in the initial value of the SYS and correspondingly different slope of the functions. However, discrepancy of the predicted maximum number of layers and de facto printed number of layers differ in the same range as with composition M-A1.

4 Conclusion

Key rheological properties of printable foam concrete were reported and the effects of substituting the cement with silica fume and alumosilicate were quantified. The foam concrete compositions M-A2 and M-A3, which contained silica fume and alumosilicate, respectively, yielded higher structuration rate than the reference mixture M-A1. In essence, all three foam concretes under investigation showed promising rheological behaviour with regard to 3D printing. However, foam concrete composition M-A3 with the addition of alumosilicate showed the highest structuration rate, likewise the highest dynamic yield stress, which are essential for retaining the form stability after extrusion. A further finding was that the theoretical approach for prediction of the structural collapse by use of experimentally determined rheological parameters underestimated the wall stability according to the 3D printing test results. Future studies on printable foam concrete should be extended on clarifying this phenomenon as well towards analysis of the reproducibility of the experimentally derived rheological parameters.

Acknowledgements. This work was funded by the Deutsche Forschungsgemeinschaft (DFG, German Research Foundation), Project Numbers 387152958 and 387095311, within the priority program SPP 2005 OPUS FLUIDUM FUTURUM – Rheology of reactive, multiscale, multiphase construction materials.

References

1. Mechtcherine, V., Nerella, V.N., Will, F., Näther, M., Otto, J., Krause, M.: Large-scale digital concrete construction – CONPrint3D concept for on-site, monolithic 3D-printing. Autom. Constr. (2019). https://doi.org/10.1016/j.autcon.2019.102933

2. Ngo, T.D., Kashani, A., Imbalzano, G., Nguyen, K.T.Q., Hui, D.: Additive manufacturing (3D printing): a review of materials, methods, applications and challenges. Compos. Part B Eng. (2018). https://doi.org/10.1016/j.compositesb.2018.02.012
3. de Schutter, G., Lesage, K., Mechtcherine, V., Nerella, V.N., Habert, G., Agusti-Juan, I.: Vision of 3D printing with concrete—technical, economic and environmental potentials. Cem. Concr. Res. (2018). https://doi.org/10.1016/j.cemconres.2018.06.001
4. Valente, M., Sibai, A., Sambucci, M.: Extrusion-based additive manufacturing of concrete products: revolutionizing and remodeling the construction industry. J. Compos. Sci. (2019). https://doi.org/10.3390/jcs3030088
5. Flatt, R.J., Wangler, T.: Editorial for special issue on digital concrete. Cem. Concr. Res. (2018). https://doi.org/10.1016/j.cemconres.2018.07.007
6. Aldridge, D.: Introduction to foamed concrete: what, why, how? Propump Engineering Ltd. (2005)
7. Falliano, D., Gugliandolo, E., De Domenico, D., Ricciardi, G.: Experimental investigation on the mechanical strength and thermal conductivity of extrudable foamed concrete and preliminary views on its potential application in 3D printed multilayer insulating panels. In: 1st International Conference on Concrete and Digital Fabrication (2019). https://doi.org/10.1007/978-3-319-99519-9
8. Ramamurthy, K., Nambiar, E.K.K., Ranjani, G.I.S.: A classification of studies on properties of foam concrete. Cem. Concr. Compos. (2009). https://doi.org/10.1016/j.cemconcomp.2009.04.006
9. Amran, Y.M.H., Farzadnia, N., Abang Ali, A.A.: Properties and applications of foamed concrete; a review. Constr. Build. Mater. (2015). https://doi.org/10.1016/j.conbuildmat.2015.10.112
10. Markin, V., Sahmenko, G., Nerella, V.N., Näther, M., Mechtcherine, V.: Investigations on the foam concrete production techniques suitable for 3D-printing with foam concrete. IOP Conf. Ser. Mater. Sci. Eng. (2019). https://doi.org/10.1088/1757-899X/660/1/012039
11. Markin, V., Nerella, V.N., Schröfl, C., Guseynova, G., Mechtcherine, V.: Material design and performance evaluation of foam concrete for digital fabrication. Materials (2019). https://doi.org/10.3390/ma12152433
12. Mechtcheirine, V., Markin, V., Will, F., Näther, M., Otto, J., Krause, M., Nerella, V.N., Schröfl, C.: CONPrint3D® Ultralight – Herstellung monolithischer, tragender, wärmedämmender Wandkonstruktionen durch additive Fertigung mit Schaumbeton. Bauingenieur 405–415 (2019)
13. Engmann, J., Servais, C., Burbidge, A.S.: Squeeze flow theory and applications to rheometry: a review. J. Non-Newton. Fluid Mech. (2005). https://doi.org/10.1016/j.jnnfm.2005.08.007
14. Roussel, N., Lanos, C.: Plastic fluid flow parameters identification using a simple squeezing test. Appl. Rheol. (2003). https://doi.org/10.1515/arh-2003-0009
15. Kniele Baumaschinen GmbH: Labormischer für die Entwicklung von Spezialbetonen. BWI-Betonwerk International, pp. 84–85 (2010)
16. Ivanova, I., Mechtcherine, V.: Possibilities and challenges of constant shear rate test for evaluation of structural build-up rate of cementitious materials. Cem. Concr. Res. (2020). https://doi.org/10.1016/j.cemconres.2020.105974
17. Nerella, V.N., Beigh, M.A.B., Fataei, S., Mechtcherine, V.: Strain-based approach for measuring structural build-up of cement pastes in the context of digital construction. Cem. Concr. Res. (2018). https://doi.org/10.1016/j.cemconres.2018.08.003

18. Ivanova, I., Mechtcherine, V.: Evaluation of structural build-up rate of cementitious materials by means of constant shear rate test: parameter study, vol. 23, pp. 209–218 (2020)
19. Roussel, N.: A thixotropy model for fresh fluid concretes: theory, validation and applications. Cem. Concr. Res. (2006). https://doi.org/10.1016/j.cemconres.2006.05.025
20. Roussel, N.: Rheological requirements for printable concretes. Cem. Concr. Res. (2018). https://doi.org/10.1016/j.cemconres.2018.04.005